

Improving the Cycling Performance of Lithium-Ion Battery Si/Graphite Anodes Using a Soluble Polyimide Binder

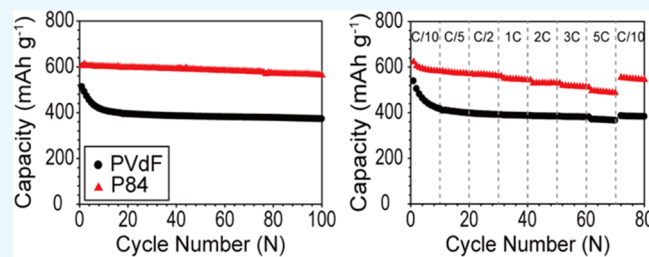
Jeonghun Oh,^{†,§} Dahee Jin,^{†,§} Kyuman Kim,[†] Danoh Song,[†] Yong Min Lee,^{*,‡} and Myung-Hyun Ryoo^{*,†,ID}

[†]Department of Chemical and Biological Engineering, Hanbat National University, 125 Dongseo-daero, Yuseong-gu, Daejeon 34158, Republic of Korea

[‡]Department of Energy Systems Engineering, Daegu Gyeongbuk Institute of Science and Technology (DGIST), 333 Techno Jungang-Daero, Daegu 42988, Republic of Korea

Supporting Information

ABSTRACT: Herein, we improved the performance of Si/graphite (Si/C) composite anodes by introducing a highly adhesive co-polyimide (P84) binder and investigated the relationship between their electrochemical and adhesion properties using the 90° peel test and a surface and interfacial cutting analysis system. Compared to those of conventional poly(vinylidene fluoride) (PVdF)-based electrodes, the cycling performance and rate capability of P84-based Si/C anodes were improved by 47.0% (372 vs 547 mAh g⁻¹ after 100 cycles at a 60 mA g⁻¹ discharge condition) and 33.4% (359 vs 479 mAh g⁻¹ after 70 cycles at a 3.0 A g⁻¹ discharge condition), respectively. Importantly, the P84-based electrodes exhibited less pronounced morphological changes and a smaller total cell resistance after cycling than the PVdF-based ones, also showing better interlayer adhesion (F_{mid}) and interfacial adhesion to Cu current collectors (F_{inter}).



INTRODUCTION

The progressing fossil fuel depletion and global climate change pose a serious threat to humankind, thus requiring internationally coordinated efforts and attention. Electric vehicles (EVs) and energy storage systems (ESS's) have gained tremendous attention as one of the promising greenhouse gasses solution.^{1–3}

However, the successful implementation of EVs and ESS's relies on high-energy-density battery systems. Although lithium-ion batteries (LIBs) based on carbon anode materials (graphite, 372 mAh g⁻¹ for LiC₆) and transition-metal-oxide cathode materials (e.g., lithium cobalt oxide, LiCoO₂) have been commercialized to power mobile electrical devices, their current energy density is still too low to satisfy the high-level requirements of large-scale applications such as EVs and ESS's.

Although silicon has received much attention as a promising anode material due to its high theoretical energy density (4200 mAh g⁻¹ for Li₂₂Si₅ or Li_{4.4}Si), environmental friendliness, and low cost,^{4–8} it has not been successfully implemented in commercialized LIBs because of suffering from large volume changes (>300%) during alloying and dealloying. Moreover, the stresses accompanying these changes cause mechanical failure and result in severely degraded electrochemical performances of Si electrodes.

Consequently, Si/graphite (Si/C) composite anodes (Si/C anodes), wherein Si constitutes only a portion of the active material, have been proposed as an alternative to pure Si anodes.^{9,10} This approach exhibits certain advantages because

even if the theoretical anode capacity increases infinitely, the total theoretical capacity of the battery soon reaches saturation because of the limited theoretical capacity of the cathode.¹¹

We have recently succeeded in enhancing the performance of Si-based anodes by using mussel-inspired and co-polyimide-based adhesive polymeric binders, hierarchical Si composites, adhesive Cu current collectors, and adhesive conductive additives.^{4,5,12,13} Still, the demand for battery-suitable high-loading Si/C-based anodes requires further progress in this direction. However, as shown in Table S1 (Supporting Information), the importance of active material loading in Si/C anodes has been underestimated by current studies.

P84 is a highly adhesive, soluble, and thermally stable co-polyimide-based binder, exhibiting outstanding intrinsic properties compared to those of conventional polymeric binders and thus improving the performances of battery constituents (anodes, cathodes, and separators), enhancing the cycling performances of Si-based anodes and the high-temperature electrochemical performances of cathode materials and increasing the thermal stability of LIBs that contain layers of ceramic composite separators.^{7,14–16}

Herein, we used P84 in high-loading Si/C-based anodes (~4.0 mg cm⁻²) and investigated their electrochemical and mechanical properties. Specifically, electrochemical properties

Received: September 13, 2017

Accepted: November 16, 2017

Published: November 29, 2017

such as electrochemical stability, cycling performance, rate capability, and impedance were evaluated using cyclic voltammetry (CV) and alternating current impedance spectroscopy, with the corresponding data recorded using a battery cycler. The mechanical properties of the above anodes were evaluated using the 90° peel test and a surface and interfacial cutting analysis system (SAICAS).

■ RESULT AND DISCUSSION

The uniformity of Si/C anodes was characterized by scanning electron microscopy (SEM) coupled with energy-dispersive X-ray spectroscopy (EDX). Figure 1 shows that the electrode

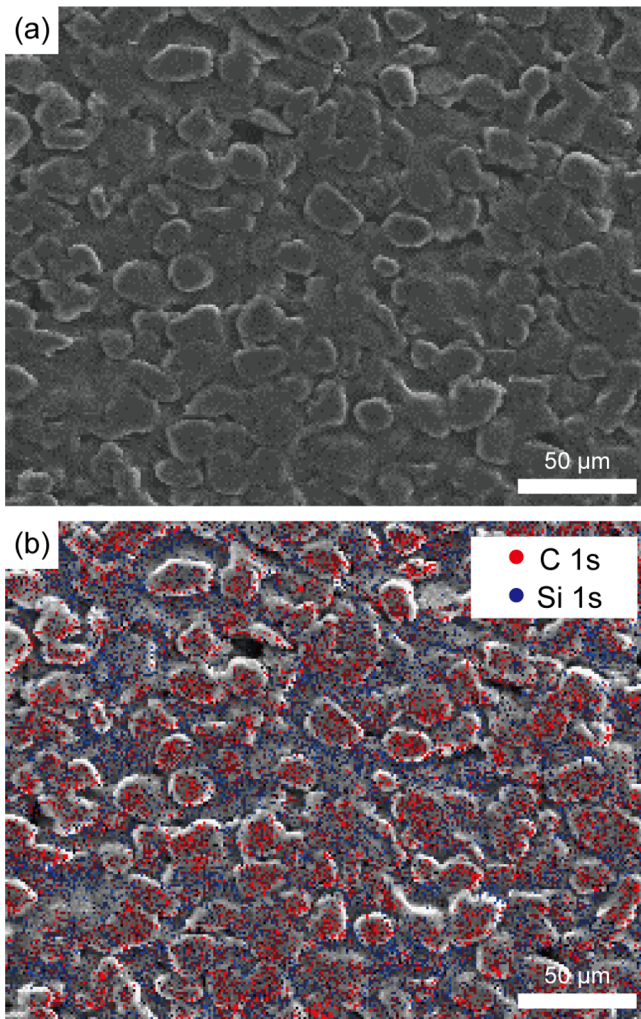


Figure 1. (a) SEM image of the P84-based Si/C anode surface and (b) EDX elemental mapping relevant to (a) (blue = Si, red = C).

surface featured uniformly distributed microsized graphite particles, with the gaps between them filled by nanosized Si, confirming that Si/C anodes exhibited good surface uniformity.

PVdF- and P84-based Si/C anodes were precycled, and the obtained results were compared. As depicted in Figure 2, P84-based Si/C showed a higher discharge capacity than that of PVdF-based Si/C (P84-based Si/C: 900.6 mAh g⁻¹ for charging and 602.5 mAh g⁻¹ for discharging; PVdF-based Si/C: 658.7 mAh g⁻¹ for charging and 523.8 mAh g⁻¹ for discharging). In contrast, the former electrode exhibited a lower Coulombic efficiency than that of the latter one (66.9 vs 79.5%,

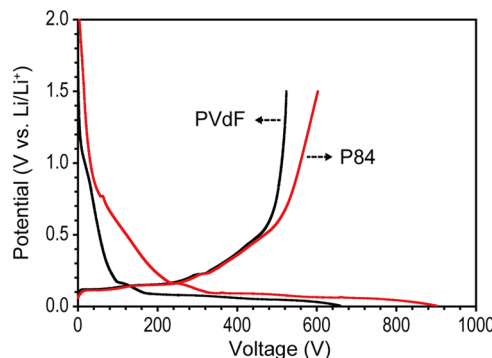


Figure 2. Potential profiles of P84- and PVdF-based Si/C anodes recorded during precycling.

respectively), which seemed to be closely related to the irreversibility of the reduction reaction, as is discussed below.

Electrochemical stabilities were probed by CV, with both electrodes showing almost identical profiles from open circuit voltage (OCV) to 0.9 V vs Li/Li⁺, whereas P84-based Si/C exhibited a more intense reduction peak below 0.9 V vs Li/Li⁺ (Figure 3). As suggested in previous studies, this behavior is

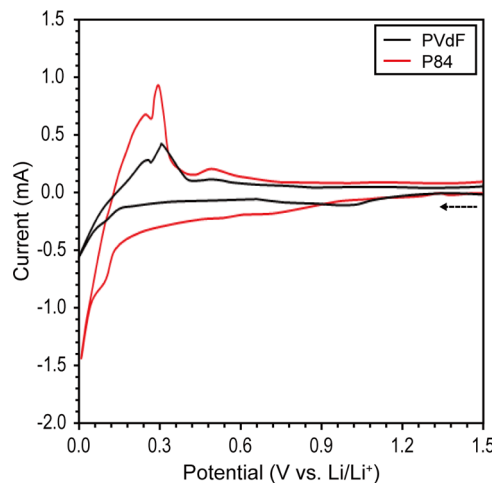


Figure 3. Cyclic voltammetry (CV) profiles of P84- and PVdF-based Si/C anodes recorded at a scan rate of 0.1 mV s⁻¹.

related to the intrinsic properties of imide-based polymeric materials, i.e., the C=O groups of the imide ring in P84 react with Li⁺ during charging.^{7,17} Interestingly, P84-based Si/C showed a stronger oxidation peak than that of PVdF-based Si/C. The above results were in good agreement with those of previous precycling tests relevant to Figure 1, revealing that P84-based Si/C showed higher discharge and charge capacities than those of PVdF-based Si/C and implying that the irreversible reduction reaction played a positive role in Si/C anodes.

CV profiles of PVdF-based Si/C anodes and P84-based Si/C anodes at 5th, 10th, 15th, and 20th scans were drawn and compared. As shown in Figure 3, the magnitude of the current peaks increased with cycling due to activation of more material to react with Li in each scan.¹⁸ Furthermore, the first scan shown in Figure 3 differs from those due to a “formation” effect, corresponding to the filming of the electrode during the first Li discharging.

For graphite anodes, the main reactions are believed to be the solvated Li intercalation (at potentials from ~ 0.8 to ~ 0.2 V vs Li/Li⁺) and the reversible formation of subsequent stages of Li_xC_6 (at potentials from ~ 0.2 to ~ 0.005 V vs Li/Li⁺).¹⁹ The stepped voltage profile of Si can be observed in a high-temperature experiment (415°C) to form four intermediate equilibrium phases. In contrast, at a mild temperature (25°C), lithiation shows a single gradually sloping plateau (~ 0.1 V vs Li/Li⁺) and large hysteresis between lithiation and delithiation.²⁰ This is because the lithiation process results in the formation of a metastable amorphous Li_xSi phase instead of the equilibrium intermetallic compounds.²⁰ Considering the overlapping voltage plateau region of graphite (~ 0.2 to ~ 0.005 V vs Li/Li⁺) and Si (~ 0.1 V vs Li/Li⁺) during lithiation, delithiation voltage plateau should be carefully considered to distinguish the role of each active material.

As depicted in Figure 4, the P84-based Si/C anodes showed two overlapping peaks at ~ 0.27 and ~ 0.32 V and a broad

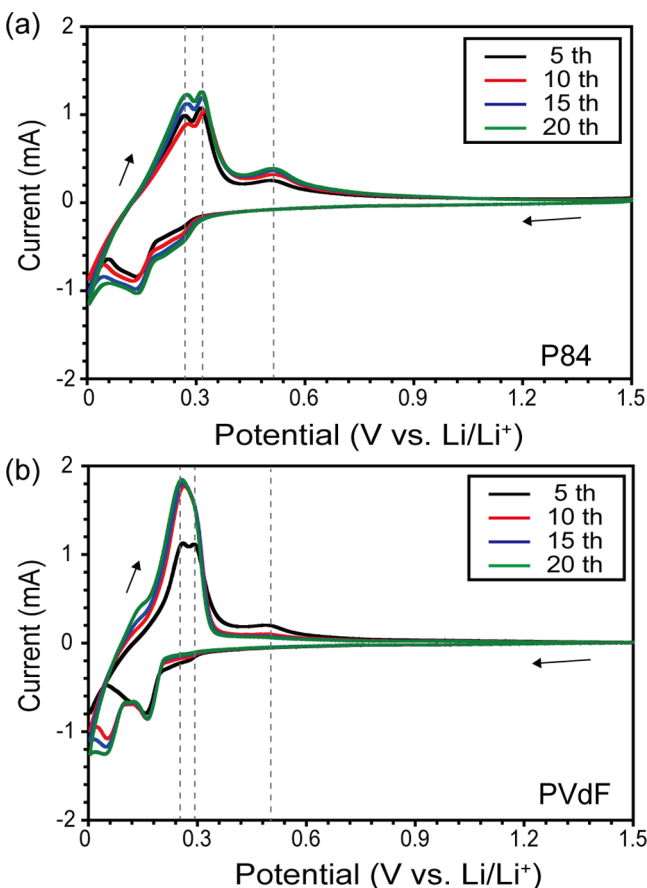


Figure 4. CV profiles of (a) P84-based Si/C anodes and (b) PVdF-based Si/C anodes during 5th, 10th, 15th, and 20th scans recorded at a scan rate of 0.1 mV s^{-1} .

shoulder peak at ~ 0.5 V during charging (delithiation) until the 20th scan. In contrast, PVdF-based Si/C showed a peak shape similar to that of the P84-based Si/C anodes up to the 5th scan and showed a single peak at ~ 0.27 V without the ~ 0.5 V wide shoulder peak from the next scan. Considering the fact that the PVdF-based Si/C showed a rapid capacity decrease due to Si pulverization (Figure 5), a long-lasting single peak at ~ 0.27 V corresponds to graphite, whereas the other peaks at ~ 0.32 and

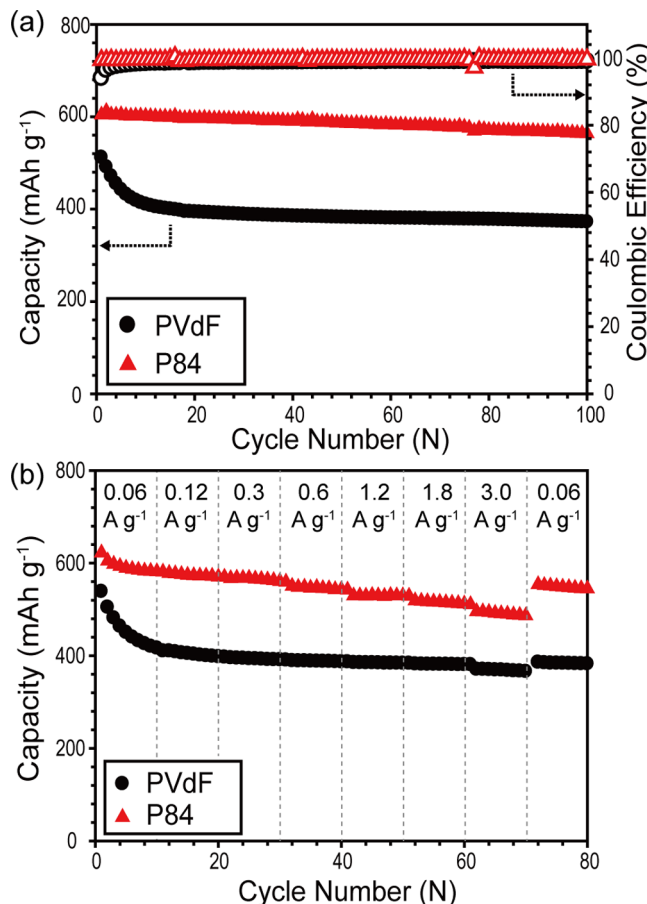


Figure 5. Electrochemical performances of P84- and PVdF-based Si/C anodes: (a) cycling performance (charge rate = 60 mA g^{-1} , discharge rate = 60 mA g^{-1}). (b) Rate capabilities determined by varying the discharge rate from 60 mA g^{-1} to 3.0 A g^{-1} while maintaining the charging rate at 60 mA g^{-1} .

~ 0.5 V correspond to Si. The peak characteristics of Si are in good agreement with those in the previous study.²¹

Subsequently, we investigated the effect of polymeric binders on the cycling performance and rate capability of Si/C anodes.

As shown in Figure 5a, P84-based Si/C showed better cycling performance than that of PVdF-based Si/C, with the respective capacity retentions after 100 cycles equaling 93 and 72% (P84-based Si/C: initial discharge capacity = 586 mAh g^{-1} , discharge capacity at 100th cycle = 547 mAh g^{-1} ; PVdF-based Si/C: initial discharge capacity = 511 mAh g^{-1} , discharge capacity at 100th cycle = 372 mAh g^{-1}). Furthermore, P84-based Si/C exhibited a capacity retention of 88% after 200 cycles (Figure S1, Supporting Information; discharge capacity at 200th cycle = 516 mAh g^{-1}).

Furthermore, we investigated the cycling performance of P84-based Si/C anodes at different active material loadings and current densities (Figure S2, Supporting Information), revealing that the electrode with the lowest loading (1.0 mg cm^{-2}) showed the best performance during high-current-density charging (0.3 A g^{-1}). In contrast, Si/C anodes with the highest loading (4.0 mg cm^{-2}) showed poor cycling performance and a low discharge capacity of $\sim 400 \text{ mAh g}^{-1}$. As depicted in Figure 5a, a low current density (60 mA g^{-1}) was required for the high-loading Si/C anodes (4.0 mg cm^{-2}) to achieve a discharge capacity ($\sim 600 \text{ mAh g}^{-1}$) exceeding that of graphite (372 mAh g^{-1}). Considering the importance of high-

loading anodes (Table S1, Supporting Information) and the fact that long-term ESS's utilize charging at a rate of C/12, one can infer that the high-loading P84-based Si/C systems with a stable cycling performance and high discharge capacity (Figure 5a, charging rate = C/10) are suitable for practical applications.^{22,23}

As shown in Figure 5b, P84-based Si/C showed a better rate capability than that of PVdF-based Si/C, with the above electrodes maintaining 81 and 70% of the initial discharge capacity, respectively, after 70 cycles at 5C (P84-based Si/C: initial discharge capacity = 586 mAh g⁻¹, discharge capacity at 70th cycle = 479 mAh g⁻¹; PVdF-based Si/C: initial discharge capacity = 511 mAh g⁻¹, discharge capacity at 70th cycle = 359 mAh g⁻¹).

After precycling, the interfacial resistances of unit cells comprising P84-based and PVdF-based Si/C anodes were measured and compared. In general, the total cell resistance (R_{total}) comprises bulk resistance (R_b), solid–electrolyte interphase (SEI) resistance (R_{SEI}), and charge transfer resistance (R_{ct}), i.e., $R_{\text{total}} = R_b + R_{\text{SEI}} + R_{\text{ct}}$.^{24–26} To explore the origin of electrochemical properties of LIB cells in practice, R_{total} should be closely monitored because, in general, the LIB cells having smaller R_{total} revealed the improved rate capability and cycle performance.^{16,26–31} As shown in Figure 6, we fitted

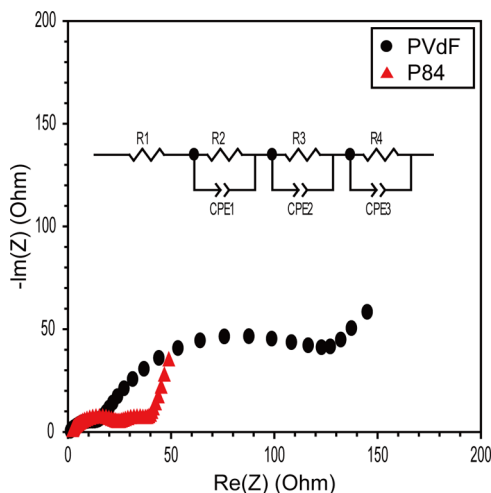


Figure 6. Impedance spectra of unit cells containing P84- and PVdF-based Si/C anodes after precycling.

the electrochemical impedance spectroscopy results using an equivalent-circuit model based on the fact that the SEI was composed of multiple layers.³² The unique feature of this model is the separation of (1) all Ohmic resistant components lumping into R_1 and (2) Faradaic nonlinear components into the R_2 , R_3 , and R_4 . To be more specific, R_1 , $(R_2 + R_3)$, and R_4 represent R_b , R_{SEI} , and R_{ct} , respectively. The calculated resistance is listed in Table S1. The R_{total} of P84-based Si/C cells was much smaller than that of PVdF-based Si/C cells, in agreement with the improved cycling performance and rate capability of the former electrodes. Taking this into account, it can be inferred that P84 effectively prevents Si pulverization and produces thin SEI layers with a smaller resistance.

As shown in Figure 7, the initial morphologies of PVdF- and P84-based Si/C anodes were different due to the inherent differences in the physical and chemical properties of constituent polymeric binders. However, the above anodes showed opposite surface morphology changes after cycling, i.e., cycled PVdF-based Si/C anodes featured larger numbers of deep big cracks than those in pristine ones, whereas cycled P84-based Si/C anodes exhibited less surface cracks than those in pristine ones. Because newly formed cracks consume large electrolyte amounts for SEI formation on the fresh active material surface and form dead active Si materials, cracking can decrease electrode capacity and increase interfacial resistance during cycling,^{33,34} in agreement with our previous experimental results discussed above.

Adhesion inside electrode composites as well as between the electrode composite and current collectors significantly affects the electrode cycling performance.^{35–38} To investigate the effect of polymeric binder type on the adhesion properties of Si/C, they were evaluated using the 90° peel test and SAICAS.

As shown in Figure 8a, P84- and PVdF-based Si/C anodes showed typical adhesion strength profiles, with the former showing a higher adhesion strength than that of the latter (0.0594 and 0.0346 kN m⁻¹, respectively).^{5,8} On the basis of Griffith's theory of cracking, however, the material fracture is originated due to the presence of microscopic flaws in the bulk material, i.e., if microscopic flaws are present in the material, the fracture stress increases and the materials can be easily fractured and/or torn apart in spite of the inherent mechanical strength.³⁹ That is, the adhesion strength measured by the peel test cannot represent the adhesion properties of the Si/C anodes properly. In view of the above, the specific adhesion properties of Si/C anodes were evaluated using SAICAS.

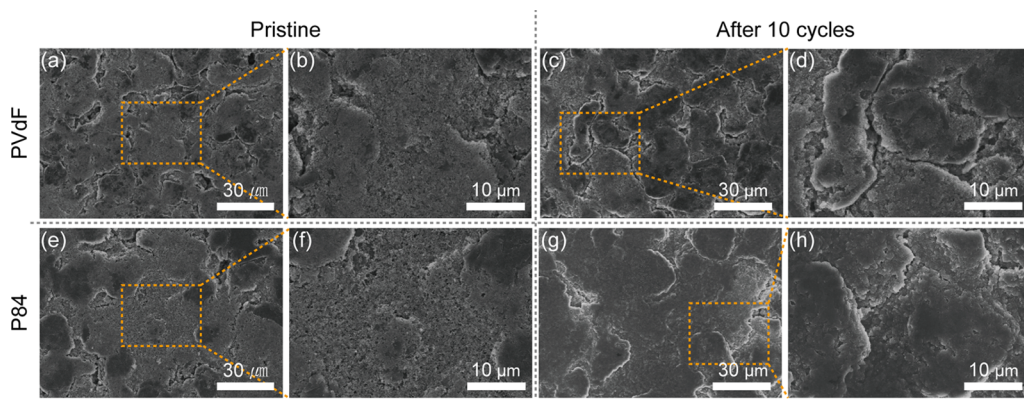


Figure 7. SEM images of the surfaces of (a–d) P84-based Si/C anodes and (e–h) PVdF-based Si/C anodes before and after the 10th cycle relevant to Figure 5a.

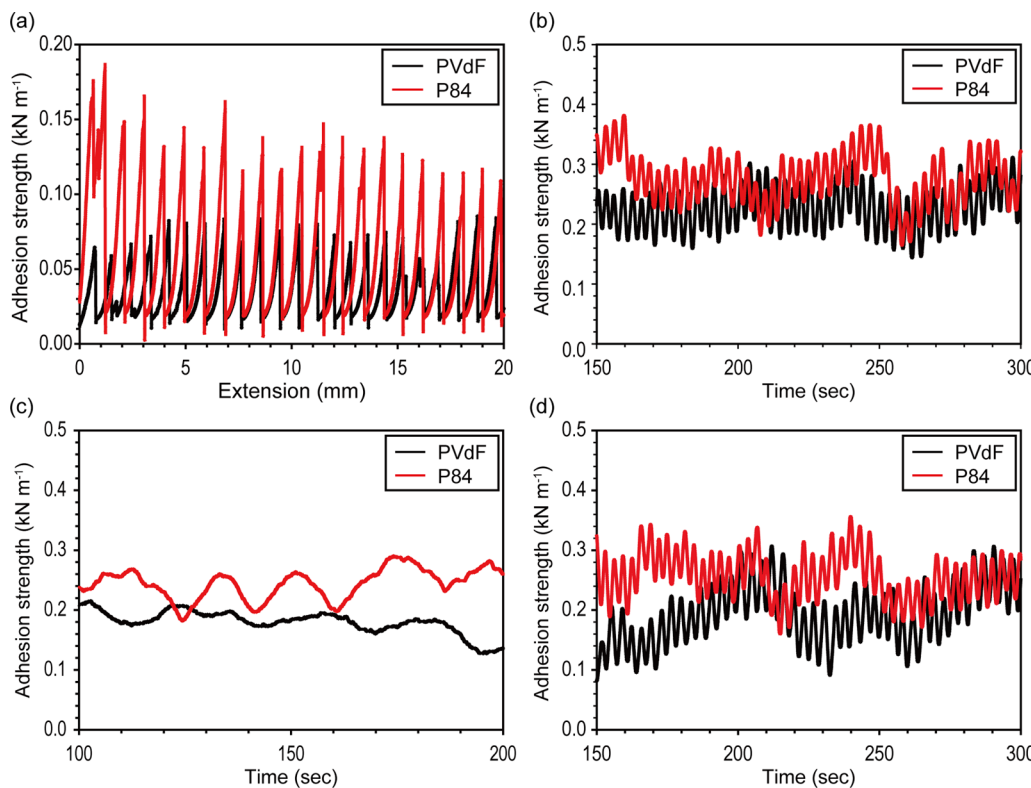


Figure 8. (a) Adhesion strength profiles of P84- and PVdF-based Si/C anodes determined by the 90° peel test. (b) Interfacial adhesion strength (F_{inter}) and (c) interlayer adhesion strength (F_{mid}) measured at $15 \mu\text{m}$ from the surface of P84- and PVdF-based Si/C anodes. (d) F_{inter} of P84- and PVdF-based Si/C anodes after 10 cycles relevant to Figure 5a.

SAICAS allows one to determine the adhesion properties of Si/C anodes at a specific position by adjusting the blade depth relative to the electrode surface. For convenience, the interlayer adhesion (F_{mid}) in Si/C composites was measured at $15 \mu\text{m}$ from the surface, with the interfacial adhesion between Si/C composites and Cu current collectors denoted F_{inter} .

As depicted in Figure 7b,c, P84-based Si/C anodes ($F_{\text{mid}} = 0.2422 \pm 0.01 \text{ kN m}^{-1}$, $F_{\text{inter}} = 0.2728 \pm 0.004 \text{ kN m}^{-1}$) showed better adhesion properties than those of PVdF-based Si/C anodes ($F_{\text{mid}} = 0.2214 \pm 0.02 \text{ kN m}^{-1}$, $F_{\text{inter}} = 0.2214 \pm 0.001 \text{ kN m}^{-1}$).

After cycling performance tests relevant to Figure 5a, both anodes were disassembled after 10 cycles and their F_{inter} values were measured and compared. In both cases, F_{inter} decreased after cycling, with this decrease being less pronounced for P84-based Si/C (92.9% of the initial F_{inter} value, from 0.2728 ± 0.004 to $0.2534 \pm 0.01 \text{ kN m}^{-1}$) than for PVdF-based Si/C anodes (83.7% of the initial F_{inter} value, from 0.2214 ± 0.001 to $0.1854 \pm 0.01 \text{ kN m}^{-1}$). This result is closely related to the larger mechanical strength of P84, which is less prone to swelling than PVdF.^{6,17}

Thus, SAICAS-determined adhesion properties revealed that the firm interlayer adhesion of the Si/C anode composite and its interfacial adhesion to Cu current collectors contributed to its enhanced performance.

CONCLUSIONS

Herein, we showed that highly adhesive and soluble copolyimide polymeric binders (e.g., P84) can improve the electrochemical properties of Si/C anodes such as cycling performance and rate capabilities, additionally facilitating the anode preparation process. Because of the inherent physical

properties of P84, P84-based Si/C anodes showed better adhesion properties (F_{mid} and F_{inter}) and less pronounced adhesion decrease upon cycling than those of PVdF-based Si/C ones, which resulted in the enhanced cycling performances and rate capabilities of the former electrodes. Moreover, P84 diminished the severe morphological changes induced by charging/discharging and achieved a smaller total cell resistance after cycling.

EXPERIMENTAL SECTION

Electrode Preparation. Si/C anodes were prepared by coating a slurry of 5 wt % Si (30–50 nm, Nanostructured & Amorphous Materials), 75 wt % graphite (CGB-20, Nippon Graphite, Japan), 10 wt % conductive carbon (Super-P Li, IMERYS, Switzerland), and 10 wt % polymeric binder in *N*-methyl-2-pyrrolidone (NMP, Sigma-Aldrich) onto Cu current collector foil (11 μm , Iljin Materials, Republic of Korea) using a doctor blade technique. Two polymeric binders were used, namely, PVdF ($M_w = 350\,000$, KF-1300, Kureha Battery Materials Co., Japan) and P84 ($M_w = 150\,000$, HP Polymer GmbH, Germany) dissolved in NMP. The cast slurry was dried in air at 80°C for 2 h and roll-pressed using a gap-control-type roll-pressing machine (CLP-2025, CIS, Republic of Korea). The loading and thickness of Si/C anodes were controlled as $\sim 4 \text{ mg cm}^{-2}$ and $30 \mu\text{m}$ in both cases.

Morphological Analysis of Si/C Anodes. The elemental distributions and surface morphologies of the prepared electrodes were examined by field emission scanning electron microscopy (MIRA LMH, TESCAN and FE-SEM, S4800, Hitachi) coupled with energy-dispersive X-ray spectroscopy (EDX; Genesis XM2, EDAX Inc.).

Cell Assembly. Si/C anodes were cut into disks (diameter = 12 mm) and assembled into 2032-type coin half-cells using Li metal (thickness = 200 μm , diameter = 16.2 mm; Honjo Metal Co., Japan) as the counter electrode. Polyethylene separators (thickness = 20 μm , diameter = 18 mm; ND420, Asahi Kasei) were employed, and 1.15 M lithium hexafluorophosphate in ethylene carbonate/diethyl carbonate (3:7, v/v) containing 5 wt % fluoroethylene carbonate (ENCHEM, Republic of Korea) was used as an electrolyte. Cell assembly was conducted in an argon-filled glove box with a dew point below -60°C .

Electrochemical Measurements. The electrochemical properties of Si/C anodes were probed by cyclic voltammetry (CV) using an impedance analyzer (VSP, Bio-Logic). The prepared 2032-type unit cells (Si/C half-cell) were scanned at a rate of 0.1 mV s^{-1} in a potential range of 0.005–1.5 V vs Li/Li $^+$, starting from the open circuit voltage (OCV).

The assembled cells were aged for 12 h and then cycled between 0.005 and 1.5 V in constant current mode at a rate of 0.06 A g^{-1} and 25°C in both charge and discharge modes using a charge/discharge cycler (PNE Solution, Republic of Korea).

After the above cycling, the total cell impedance was measured using an impedance analyzer (VSP, Bio-Logic) in a frequency range of 1 MHz to 0.01 Hz.

To evaluate the cycling performance, cells were subjected to 100 cycles at a current density of 0.06 A g^{-1} at 25°C . Furthermore, to evaluate rate capabilities, the discharge current densities were varied from 0.06 to 3 A g^{-1} , with the charging current density maintained at 0.06 A g^{-1} .

90° Peel Test. A 20 mm \times 20 mm anode sample was attached to 3 M adhesive tape, and peel strength was measured using a micro material tester (Instron 5848, Instron Company). The adhesive tape was removed by peeling at an angle of 90° and a constant displacement rate of 10 mm min^{-1} , with the applied load being continuously measured to construct force/displacement plots.

SAICAS Measurements. The interlayer adhesion of the Si/C composite (F_{mid}) and the interfacial adhesion between Si/C anodes and Cu current collectors (F_{inter}) were characterized by SAICAS (Daipla Wintes Co., Ltd.) utilizing a 1 mm wide boron nitride blade fixed at a shear angle of 45° . For measuring F_{mid} the blade was positioned 15 μm from the anode surface. During the test, the blade moved in the horizontal direction at 0.2 $\mu\text{m s}^{-1}$, maintaining a vertical force of 0.2 N.

■ ASSOCIATED CONTENT

Supporting Information

The Supporting Information is available free of charge on the ACS Publications website at DOI: [10.1021/acsomega.7b01365](https://doi.org/10.1021/acsomega.7b01365).

Comparison table of current work with state-of-the-art work on Si/C anode electrodes and the electrochemical performance of Si/C anodes at different active material loadings and current densities ([PDF](#))

■ AUTHOR INFORMATION

Corresponding Authors

*E-mail: yongmin.lee@hanbat.ac.kr. Tel.: +53-785-6425. Fax: +82-53-785-6409 (Y.M.L.).

*E-mail: mhryou@hanbat.ac.kr. Tel./Fax: +82-42-821-1534 (M.-H.R.).

ORCID

Myung-Hyun Ryou: [0000-0001-8899-019X](http://orcid.org/0000-0001-8899-019X)

Author Contributions

[§]J.O. and D.J. contributed equally to this work.

Notes

The authors declare no competing financial interest.

■ ACKNOWLEDGMENTS

This work was supported by the Human Resource Training Program for Regional Innovation and Creativity through the Ministry of Education and National Research Foundation of Korea (NRF-2014H1C1A1066977). This work was also supported by New Product Development Project under Purchase Condition (Domestic) funded by the Small and Medium Business Administration of Korea (S2439826).

■ REFERENCES

- (1) Li, Y.; Yang, J.; Song, J. Design Principles and Energy System Scale Analysis Technologies of New Lithium-Ion and Aluminum-Ion Batteries for Sustainable Energy Electric Vehicles. *Renewable Sustainable Energy Rev.* **2017**, *71*, 645–651.
- (2) Tie, S. F.; Tan, C. W. A Review of Energy Sources and Energy Management System in Electric Vehicles. *Renewable Sustainable Energy Rev.* **2013**, *20*, 82–102.
- (3) Larcher, D.; Tarascon, J.-M. Towards Greener and More Sustainable Batteries for Electrical Energy Storage. *Nat. Chem.* **2015**, *7*, 19–29.
- (4) Song, D.; Jung, D.; Cho, I.; Ryou, M. H.; Lee, Y. M. Mussel-Inspired Polydopamine-Functionalized Super-P as a Conductive Additive for High-Performance Silicon Anodes. *Adv. Mater. Interfaces* **2016**, *3*, No. 1600270.
- (5) Ryou, M.-H.; Kim, J.; Lee, I.; Kim, S.; Jeong, Y. K.; Hong, S.; Ryu, J. H.; Kim, T. S.; Park, J. K.; Lee, H.; et al. Mussel-Inspired Adhesive Binders for High-Performance Silicon Nanoparticle Anodes in Lithium-Ion Batteries. *Adv. Mater.* **2013**, *25*, 1571–1576.
- (6) Koo, B.; Kim, H.; Cho, Y.; Lee, K. T.; Choi, N. S.; Cho, J. A Highly Cross-Linked Polymeric Binder for High-Performance Silicon Negative Electrodes in Lithium Ion Batteries. *Angew. Chem., Int. Ed.* **2012**, *51*, 8762–8767.
- (7) Choi, J.; Kim, K.; Jeong, J.; Cho, K. Y.; Ryou, M.-H.; Lee, Y. M. Highly Adhesive and Soluble Copolyimide Binder: Improving the Long-Term Cycle Life of Silicon Anodes in Lithium-Ion Batteries. *ACS Appl. Mater. Interfaces* **2015**, *7*, 14851–14858.
- (8) Jeong, Y. K.; Kwon, T.-W.; Lee, I.; Kim, T.-S.; Coskun, A.; Choi, J. W. Hyperbranched β -Cyclodextrin Polymer as an Effective Multidimensional Binder for Silicon Anodes in Lithium Rechargeable Batteries. *Nano Lett.* **2014**, *14*, 864–870.
- (9) Yim, C.-H.; Courtel, F. M.; Abu-Lebdeh, Y. A High Capacity Silicon–Graphite Composite as Anode for Lithium-Ion Batteries Using Low Content Amorphous Silicon and Compatible Binders. *J. Mater. Chem. A* **2013**, *1*, 8234–8243.
- (10) Yim, C.-H.; Niketic, S.; Salem, N.; Naboka, O.; Abu-Lebdeh, Y. Towards Improving the Practical Energy Density of Li-Ion Batteries: Optimization and Evaluation of Silicon: Graphite Composites in Full Cells. *J. Electrochem. Soc.* **2017**, *164*, A6294–A6302.
- (11) Yoshio, M.; Tsumura, T.; Dimov, N. Electrochemical Behaviors of Silicon based Anode Material. *J. Power Sources* **2005**, *146*, 10–14.
- (12) Jung, D. S.; Ryou, M.-H.; Sung, Y. J.; Park, S. B.; Choi, J. W. Recycling Rice Husks for High-Capacity Lithium Battery Anodes. *Proc. Natl. Acad. Sci. U.S.A.* **2013**, *110*, 12229–12234.
- (13) Cho, I.; Gong, S.; Song, D.; Lee, Y.-G.; Ryou, M.-H.; Lee, Y. M. Mussel-Inspired Polydopamine-Treated Copper Foil as a Current Collector for High-Performance Silicon Anodes. *Sci. Rep.* **2016**, *6*, No. 30945.
- (14) Choi, J.; Ryou, M.-H.; Son, B.; Song, J.; Park, J.-K.; Cho, K. Y.; Lee, Y. M. Improved High-Temperature Performance of Lithium-Ion Batteries Through Use of a Thermally Stable Co-Polyimide-Based Cathode Binder. *J. Power Sources* **2014**, *252*, 138–143.

- (15) Song, J.; Ryou, M.-H.; Son, B.; Lee, J.-N.; Lee, D. J.; Lee, Y. M.; Choi, J. W.; Park, J.-K. Co-Polyimide-Coated Polyethylene Separators for Enhanced Thermal Stability of Lithium Ion Batteries. *Electrochim. Acta* **2012**, *85*, 524–530.
- (16) Kim, J.-H.; Kim, J. H.; Kim, J. M.; Lee, Y. G.; Lee, S. Y. Superlattice Crystals—Mimic, Flexible/Functional Ceramic Membranes: Beyond Polymeric Battery Separators. *Adv. Energy Mater.* **2015**, *5*, No. 1500954.
- (17) Choi, N.-S.; Yew, K. H.; Choi, W.-U.; Kim, S.-S. Enhanced Electrochemical Properties of a Si-based Anode Using an Electrochemically Active Polyamide Imide Binder. *J. Power Sources* **2008**, *177*, 590–594.
- (18) Chan, C. K.; Peng, H.; Liu, G.; McIlwrath, K.; Zhang, X. F.; Huggins, R. A.; Cui, Y. High-Performance Lithium Battery Anodes Using Silicon Nanowires. *Nat. Nanotechnol.* **2008**, *3*, 31–35.
- (19) Winter, M.; Novák, P.; Monnier, A. Graphites for Lithium-Ion Cells: The Correlation of the First-Cycle Charge Loss with the Brunauer-Emmett-Teller Surface Area. *J. Electrochem. Soc.* **1998**, *145*, 428–436.
- (20) McDowell, M. T.; Lee, S. W.; Nix, W. D.; Cui, Y. 25th Anniversary Article: Understanding the Lithiation of Silicon and Other Alloying Anodes for Lithium-Ion Batteries. *Adv. Mater.* **2013**, *25*, 4966–4985.
- (21) Green, M.; Fielder, E.; Scrosati, B.; Wachtler, M.; Moreno, J. S. Structured Silicon Anodes for Lithium Battery Applications. *Electrochem. Solid-State Lett.* **2003**, *6*, A75–A79.
- (22) Bray, K. L.; Conover, D. R.; Kintner-Meyer, M. C.; Viswanathan, V.; Ferreira, S.; Rose, D.; Schoenwald, D. *Protocol for Uniformly Measuring and Expressing the Performance of Energy Storage Systems*; PNNL-22010; Pacific Northwest National Laboratory (PNNL): Richland, WA, 2012.
- (23) Bussar, C.; Moos, M.; Alvarez, R.; Wolf, P.; Thien, T.; Chen, H.; Cai, Z.; Leuthold, M.; Sauer, D. U.; Moser, A. Optimal Allocation and Capacity of Energy Storage Systems in a Future European Power System with 100% Renewable Energy Generation. *Energy Procedia* **2014**, *46*, 40–47.
- (24) Lee, H.; Jeon, H.; Gong, S.; Ryou, M.-H.; Lee, Y. M. A Facile Method to Enhance the Uniformity and Adhesion Properties of Water-Based Ceramic Coating Layers on Hydrophobic Polyethylene Separators. *Appl. Surf. Sci.* **2018**, *427*, 139–146.
- (25) Lee, J.-N.; Han, G.-B.; Ryou, M.-H.; Lee, D. J.; Song, J.; Choi, J. W.; Park, J.-K. N-(Triphenylphosphoranylidene) Aniline as a Novel Electrolyte Additive for High Voltage LiCoO₂ Operations in Lithium Ion Batteries. *Electrochim. Acta* **2011**, *56*, 5195–5200.
- (26) Ryou, M. H.; Lee, Y. M.; Park, J. K.; Choi, J. W. Mussel-inspired Polydopamine-treated Polyethylene Separators for High-power Li-ion Batteries. *Adv. Mater.* **2011**, *23*, 3066–3070.
- (27) Lee, Y.-S.; Jeong, Y. B.; Kim, D.-W. Cycling Performance of Lithium-ion Batteries Assembled with a Hybrid Composite Membrane Prepared by an Electrospinning Method. *J. Power Sources* **2010**, *195*, 6197–6201.
- (28) Liu, Q.; Xia, M.; Chen, J.; Tao, Y.; Wang, Y.; Liu, K.; Li, M.; Wang, W.; Wang, D. High Performance hybrid Al₂O₃/Poly(vinyl alcohol-co-ethylene) Nanofibrous Membrane for Lithium-ion Battery Separator. *Electrochim. Acta* **2015**, *176*, 949–955.
- (29) Liang, X.; Yang, Y.; Jin, X.; Huang, Z.; Kang, F. The High Performances of SiO₂/Al₂O₃-coated Electrospun Polyimide Fibrous Separator for Lithium-ion Battery. *J. Membr. Sci.* **2015**, *493*, 1–7.
- (30) Lee, Y.; Ryou, M.-H.; Seo, M.; Choi, J. W.; Lee, Y. M. Effect of Polydopamine Surface Coating on Polyethylene Separators as a Function of Their Porosity for High-power Li-ion Batteries. *Electrochim. Acta* **2013**, *113*, 433–438.
- (31) Choi, E.-S.; Lee, S.-Y. Particle Size-dependent, Tunable Porous Structure of a SiO₂/Poly(vinylidene fluoride-hexafluoropropylene)-coated Poly(ethylene terephthalate) Nonwoven Composite Separator for a Lithium-ion Battery. *J. Mater. Chem.* **2011**, *21*, 14747–14754.
- (32) Markovsky, B.; Levi, M. D.; Aurbach, D. The Basic Electroanalytical Behavior of Practical Graphite–Lithium Intercalation Electrodes. *Electrochim. Acta* **1998**, *43*, 2287–2304.
- (33) Winter, M.; Besenhard, J. O. Electrochemical Lithiation of Tin and Tin-Based Intermetallics and Composites. *Electrochim. Acta* **1999**, *45*, 31–50.
- (34) Wachtler, M.; Besenhard, J. O.; Winter, M. Tin and Tin-based Intermetallics as New Anode Materials for Lithium-Ion Cells. *J. Power Sources* **2001**, *94*, 189–193.
- (35) Choi, S.; Kim, J.; Eom, M.; Meng, X.; Shin, D. Application of a Carbon Nanotube (CNT) Sheet as a Current Collector for All-Solid-State Lithium Batteries. *J. Power Sources* **2015**, *299*, 70–75.
- (36) Baunach, M.; Jaiser, S.; Schmelzle, S.; Nirschl, H.; Scharfer, P.; Schabel, W. Delamination Behavior of Lithium-Ion Battery Anodes: Influence of Drying Temperature During Electrode Processing. *Drying Technol.* **2016**, *34*, 462–473.
- (37) Reyter, D.; Rousselot, S.; Mazouzi, D.; Gauthier, M.; Moreau, P.; Lestriez, B.; Guyomard, D.; Roué, L. An Electrochemically Roughened Cu Current Collector for Si-Based Electrode in Li-Ion Batteries. *J. Power Sources* **2013**, *239*, 308–314.
- (38) Wu, J.; Zhu, Z.; Zhang, H.; Fu, H.; Li, H.; Wang, A.; Zhang, H.; Hu, Z. Improved Electrochemical Performance of the Silicon/Graphite-Tin Composite Anode Material by Modifying the Surface Morphology of the Cu Current Collector. *Electrochim. Acta* **2014**, *146*, 322–327.
- (39) Jeon, H.; Choi, J.; Ryou, M.-H.; Lee, Y. M. Comparative Study of the Adhesion Properties of Ceramic Composite Separators Using a Surface and Interfacial Cutting Analysis System for Lithium-Ion Batteries. *ACS Omega* **2017**, *2*, 2159–2164.